Est. 1984

ORIENTAL JOURNAL OF CHEMISTRY

An International Open Access, Peer Reviewed Research Journal

www.orientjchem.org

ISSN: 0970-020 X
CODEN: OJCHEG
2023, Vol. 39, No.(6):
Pg. 1469-1478

Synthesis and Characterization of Copper Alumino Silicate Nanocomposites by Co-precipitation for Catalytic activity

C. VIJAYARAJ[1]*, G. NEDUNCHEZIAN[2], S. SOFIYA LAWRENCE MARY[3], and R. SUBRAMANIAN[4]

[1]*Department of Chemistry, Thiru. Vi. Ka. Government Arts College, Thiruvarur, 610003. Affiliated to Bharathidasan University, Tiruchirappalli-24, TamilNadu, India.
[2]Department of Physics, Thiru. Vi. Ka. Government Arts College, Thiruvarur, 610003. Affiliated to Bharathidasan University, Tiruchirappalli-24, Tamil Nadu,India.
[3]Department of Chemistry,Bharathidasan Govt.College forWomen,Muthialpet, Puducherry-3, Affiliated to Pondicherry University,Puducherry, India.
[4]Department of Chemistry,Sun Arts and Science College,Thiruvannamalai, TamilNadu, India.
*Corresponding author E-mail: cmvijaychem@gmail.com

http://dx.doi.org/10.13005/ojc/390607

(Received: October 26, 2023; Accepted: December 04, 2023)

ABSTRACT

Water contamination by organic dyes has become a reason for severe environmental pollution and has been threatening the aquatic ecosystem. In this present report two distinct types of copper aluminosilicate (CAS) composites to be utilized as a decreased trigger have been created by incorporating copper nanoparticles through a mesoporous aluminosilicate structure generated through a co-precipitation strategy, accompanied by calcinations at a range of conditions lacking the use of patterns. the thermal inquires, Fourier transform infrared (FT-IR) spectroscopy, XRD (X-ray diffraction) of powder estimation, microscopy using scanning electron microscopy (SEM), and the analysis of energy dispersive X-rays (EDAX) were carried out to analyze the nanocomposites that have been described earlier. The catalytic reduction tests confirmed the importance of Aluminosilicate and the high catalytic activities of the synthesized Cu/Aluminosilicate composite toward nitrophenol reduction. The kinetic analysis of the nitrophenol reduction of the catalyst has fitted the pseudo-first-order kinetic model. More than 99% removal efficiency was still present, demonstrating exceptional stability of the composite. In conclusion, the Cu/Aluminosilicate NPs composite was found to be a promising catalyst for the excellent catalytic activity to reduce a model pollutant nitrophenol from the aqueous solution in the presence of $NaBH_4$ with catalytic efficiency higher than 99% and a reduction rate constant, k_{red}, higher than 0.86 min^{-1} respectively.

Keywords: Copper aluminosilicate, Heterogeneous catalysis, Reduction, Amino phenol.

INTRODUCTION

In recent years, one issue that has generated significant concern due to its adverse effects, mainly on human health, is the contamination of water (surface and groundwater), including the ocean. The principal cause of this event is the high amounts of toxic and refractory pollutants, mainly 4-nitrophenol (4-NP), which is widely used in the pharmaceutical and textile industries, for the production of herbicides, insecticides, synthetic dyes, and paints, and as a corrosion inhibitor and pH indicator, among other applications. Therefore, the reduction of 4-NP to 4-aminophenol (4-AP) has become a crucial issue, given that 4-AP is a compound with a lower degree of toxicity. Among the various 4-NP reduction reactions, the reaction with sodium borohydride ($NaBH_4$) as a reducing agent (H2 source) in conjunction with metal catalysts, such as Pd, Ag, Pt, Cu, Au and their assemblies on dendrimers, polymeric matrices, microgels, metal-immobilized silica-coated supports, and graphene oxide[1-6]. And functionalities were introduced into mesoporous silicas and exhibited higher reduction activity compared with conventional metal-based catalysts. The catalytic activity of metal-based mesoporous silicas is dependent on the size and dispersive extent of metal NPs.

Because of the distinctive attributes of ridiculous area of coverage and granular features, nanostructured substances have drawn a lot attention for their potential as catalyst. Although nanoparticles have advantages over for diverse catalysts, that they frequently require further assistance to accomplish the heat reliability. The components such as TiO_2, Al_2O_3, SiO_2, zeolites/aluminosilicates, Chitosan, nanotubes made from carbon, and many others have been employed to be nanocatalyst supports.

In the group of these elements, aluminosilicates are commonly employed as the catalysts and as structural support for a variety of processes. The resulting condensation of tetrahedral aluminate with silicate combinations through the corners of those groups produce an aluminosilicate within a framework. A reduction in the molecular proportion of SiO_2/Al_2O_3 in the structural component triggers a boost in the ion exchange processes the capability which in turn increases the highest permissible loading of transition metal ions can be achieved[7], and a corresponding reduction in the molecules amount of SiO_2/Al_2O_3 in the structure results to an increase in the ion-exchange capacity and thus the highest possible importing of the change metal ions[8]. Although there have been many approaches that can be utilized for preparing various kinds of aluminosilicates, that include sol-gel, co-precipitation, substitutes hydrothermal heating directions, and so on, the co-precipitating methodology acts as one of the frontier techniques commonly utilized for the production of identical silicates of aluminum by organic precursors at a significantly lower heat[9]. Nanocomposite technology materials are formed while a nanosized particles element gets dispersed on an unstructured or crystallized matrix of the previously mentioned forms. Nanocomposites have become recognized as intriguing materials due to their many potential applications based on increased physical as well as chemical features[10]. The integration of transitioning metal nanoparticles/metal oxides on aluminosilicates is of major significance because it combines the aluminosilicates' high porosity and wide surface area along with the catalytic features of nanoparticles made of metal or metal oxide and can be accomplished through an effortless impermeability technique. Metal-based catalysts have long been researched as the most effective platforms for the process of hydrogenation dehydrogenation, hydrocyanation, as well as the isomerization processes, and they are more potent in the nanoscale. Copper aluminosilicate (CAS) has generated interest among silica-based materials due to its nanoporous structure, high specific surface area, and outstanding optical characteristics, making it potentially suitable for a variety of applications[11-12]. Metal nanoparticles have been extensively studied for the transfer hydrogenation of carbonyl compounds and olefins to their corresponding alcohols and alkanes, respectively[13-14]. However, the use of nanoparticles without a support will lead to agglomeration of the active catalyst and also difficulty in separation from the reaction mixture[15-16]. In order to increase the life time of the catalyst, it is necessary to stabilize the nano catalyst from agglomeration and it is expected that the loading of nanoparticles on the aluminosilicate framework will increase the catalytic activity due to the additional porous nature and acidity of the support.

In this context, we present the preparation and characterization of mesoporous copper aluminosilicate nanocomposites through co precipitation method for successfully used for the reduction of 4-nitrophenol (4-NP) to 4-aminophenol.

EXPERIMENTAL

Materials

Every single reagent had been 100% pure chemically as well as AR standard. Each of those compounds utilized consisted of both analytical and solution standards. Tetraethyl orthosilicate (TEOS) and the chloride of aluminum were procured by Aldrich and utilized with no any further purification. Cu $(NO_3)_2.6H_2O$ and hydrazine dihydrochloride had been bought at LobaChemicoPvt.Ltd. as well as used when obtained. The research study was carried out using water that had been double-distilled.

Preparation of catalyst

In such a situation, the method starts out with the dissolution of 4.38 g of $Cu(NO_3)_2.6H_2O$, 0.16 g of Na_2CO_3, with 2.00 g of anhydrous $AlCl_3$ in 60 mL dichloromethane using a cylindrical flask with a round bottom. Without delay, 6 mL of undiluted ammonia was incorporated, afterwards adding 4.75 mL of TEOS. During that stage, the jellification combination was inspected following 40 mL of water and 9 mL of ammonia were poured. The combination of ingredients has a pH of 11.0. For 24 h the combination has been maintained about 40-60°C with electromagnetic stirring within conditions conducive to reflux. The product that resulted was referred to as MAS (Metal-Aluminosilicate Produced by Co-Precipitation Method), after which it had been washed, dried, as well as calcined about 600°C and 800°C temperature. The resulting substances have been designated as MAS-6 and MAS-8. In accordance with the previous procedure, a comparison analysis had been done in without the presence of the metal copper; the air-dried solids acquired have been labeled as AS -6 and AS-8.

Characterization of catalyst

The presence of aluminosilicates and aluminosilicates that contained copper itself was discovered through the Fourier transform of the infrared spectroscopic (FT-IR) methodology. Before commencing the process of recording the spectra for the sample that is unidentified, the equipment's computer software is displayed as well as the necessary settings such as recording ranges (4000-400 cm^{-1}) have been supplied.The powder form diffraction patterns from X-rays of nanocrystals can be generated by employing an X'PERT Panalytical X-ray diffractometer (X-ray diffract (Cu-Kα radiation γ = 1.54056°A) having a speed of scanning of 0.02°/sin2θ rangein an orientation of 10° to 90°. SEM has been frequently utilized for analyzing the surfaces, frameworks, morphologies, including patterns of substances. The scanning electron microscope (SEM) examination has been carried out in an atmosphere of vacuum. Images obtained from SEM have been used to analyze the surface morphology of Cu-aluminosilicate nanocrystals. SEM snapshots had been taken using a JEOL JSM 6390 SEM that used a 15 kV expediting voltage. The molecular structure of copper aluminosilicate granules can be accurately measured with EDX technique. The basics compositional variation data applicable to an extensive category of substances is provided by way of the EDX features. To discover the precisely determined chemical makeup of an element, the emission spectrum of the EDX of copper aluminosilicate nanoparticle has been captured by using a JEOL JSM 6390 SEM appliances with thermal EDX attachment around a 15 kV acceleration of voltage.

Catalytic reduction of 4-nitrophenol to 4-aminophenol

The steps involved in the conversion of 4-nitrophenol to 4-aminophenol have been observed through ultraviolet-visible (UV-Vis) spectroscopy in an UV-Vis quartz cuvette using a path length of 1 cm, whereas the catalytic efficiency of Cu-aluminosilicate nanoparticles that has been assessed through the observation of their reaction kinetics with UV-Vis spectroscopy. A conventional process had been carried out. 2 mL of 10^{-4} (M) 4-nitrophenol mixture has been combined with 20 µL of hydrazine fluid produced in a UV-Vis cuvette by crumbling 2 mg of hydrazine in 5 mL of redistilled water. once you have completed that, 20 µL of synthesized Cu-aluminosilicate nanoparticles mixture was then incorporated to the combination, in addition ultraviolet (UV)-Visible spectra over the frequency range of 200-900 nm at 27°C have been obtained at 5-minute periods of time[17,18].

RESULTS AND DISCUSSION

Figure 1 presents the IR spectrum of the aluminosilicate base and the copper-containing catalysts as well. The apparent existence of a group with the formula -OH on the aluminosilicate interface can be determined by an extensive range in the spectrum of the FT-IR within 3100 cm^{-1} to 3700 cm^{-1}. The groups made up of silanol (Si-OH) of aluminosilicates trigger this elongation. TO_4 (in which T= Si, Al) asymmetrical vibrations caused by stretching in the inner tetrahedral have been accountable for the range of frequencies detected within 950 to 1250 cm^{-1}. The bands that lie between 650 and 800 cm^{-1} as well as 420 and 500 cm^{-1} may be triggered by symmetric stretching along with the TO4 bending mechanism of internal tetrahedral.The AS-6 FT-IR spectrum (Fig. 1A) demonstrates asymmetrical stretching of TO_4 at 1096 cm^{-1} as well as symmetrical stretching of TO_4 at 654 cm^{-1}. The circular region around 470.56 cm^{-1} in AS-6 is produced by tetrahedral bending. AS-8's FT-IR spectra (Fig. 1B) illustrates asymmetrical TO_4 stretching at 1099 cm^{-1} as well as symmetrical TO_4 stretching at 655.38 cm^{-1}. The band at 471.43 cm^{-1} in AS-8 is caused by tetrahedral bending. Additionally, loading copper into the aluminosilicate tetrahedral structure led to a minor reduction in both the stretching and bending oscillations of the tetrahedral elements, which provided some illumination on the presence of copper on the aluminosilicate framework's tetrahedral platforms. MAS-6's FT-IR spectra (Fig. 1C) indicates asymmetry lengthening of TO_4 at 1088 cm^{-1} as well as symmetry lengthening of TO4 about 653 cm^{-1}. The band that exists at 465 cm^{-1} in MAS-6 is a consequence of tetrahedral bending. MAS-8's FT-IR spectra (Fig. 1D) exhibits asymmetrical stretching of TO_4 at 1085 cm^{-1} as well as symmetrical stretching of TO_4 at 650 cm^{-1}. The band observed at 470 cm^{-1} in MAS-8 is a consequence of tetrahedral bending. As a result, the infrared spectral measurements demonstrated that copper has been integrated onto the aluminosilicate framework's tetrahedral points[19,20].

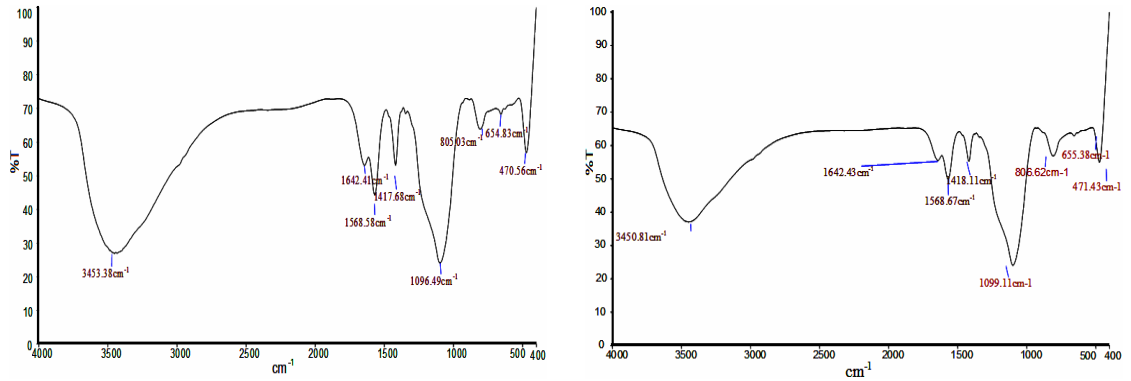

Fig. 1(a). FT-IR Spectrum of AS-6 and (b) FT IR Spectrum of AS-8 via co-precipitation method

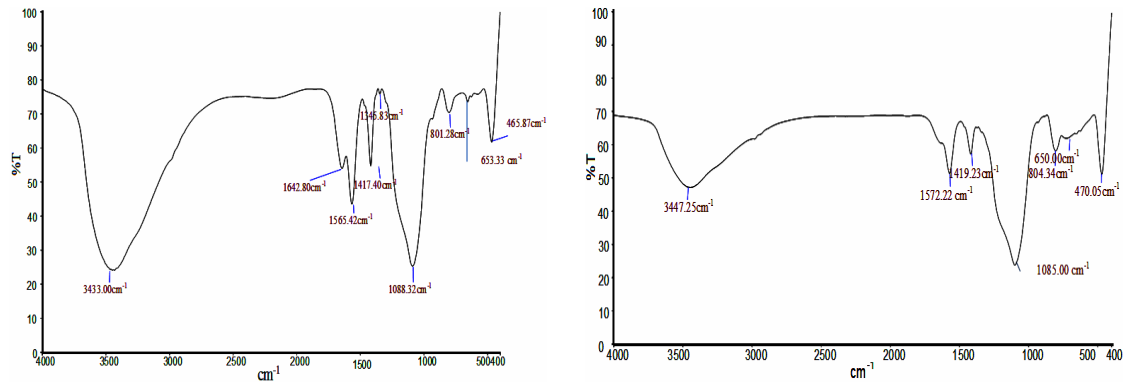

Fig. 1(c). FT -IR Spectrum of MAS-6 (d) FT-IR Spectrum of MAS-8 via co-precipitation method

SEM analysis has proven to be extremely valuable in analyzing the surface characteristics of substances. Images from the scanning electron microscope have been used for assessing the surface shape as well as porosity of both the nanoparticle catalysts MAS-6 and MAS-8. The tiered porous architecture of the catalysts featuring a big although shallow pore size and strands in each fold of the catalyst have been determined using scanning electron microscope (SEM) images (Fig. 2 A-B). It additionally exhibits the uneven forms and textures of the Cu-aluminosilicate nanoparticles[21].

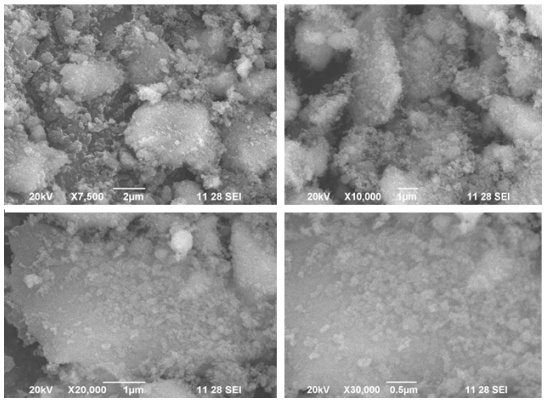

Fig. 2(a). SEM profile of MAS-6 composites by co-precipitation method

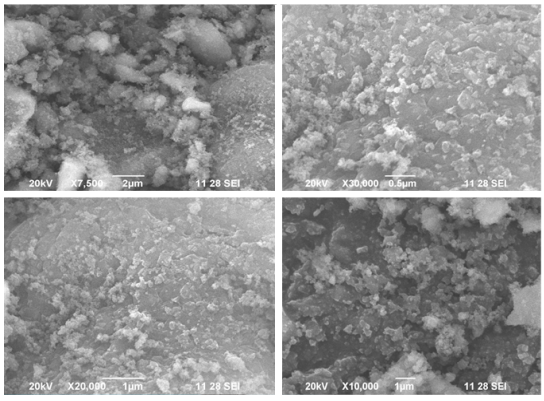

Fig. 2(b). SEM profile of MAS-8 composites by co-precipitation method

The EDX elemental analysis results presented in Table 1 unambiguously demonstrates the existence of these essential elements as well as the compounds of the substances at two distinct temperatures for calcination (Fig. 3 A-B). The volume of copper placed on the aluminosilicates reduced consistently as the proportion of aluminum to silicon on the surface and temperature at which they were calcined increased. In generally, non-crystalline encourages have greater exchange of ions power than crystalline materials, whereas crystalline structure is able to be regulated through calcining temperature, as proven by the percentage of copper reducing according to rising calcination temperature as well as the proportion of Si to Al increasing with rising calcining the temperature.

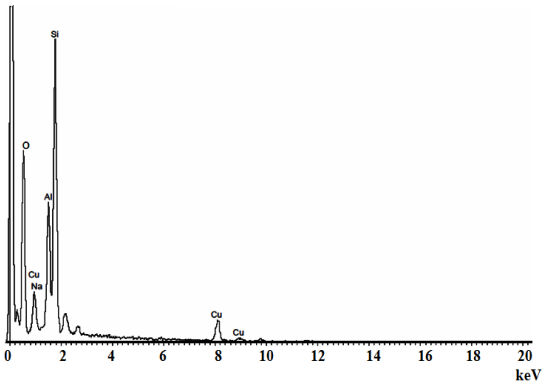

Fig. 3(a). EDX spectrum of MAS-6 composites

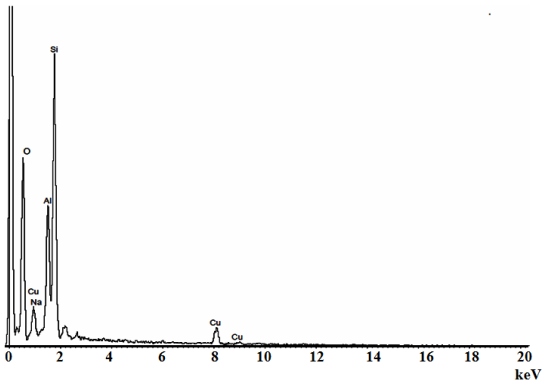

Fig. 3(b). EDX spectrum of MAS-8 composites

Table 1: Elemental composition of Cu-aluminosilicate nanoparticles

Sample	Si mass (%)	Al mass (%)	Cu mass (%)	O mass (%)	Na mass (%)
MAS 6	58.26	11.10	5.11	23.79	1.75
MAS 8	62.29	9.59	3.02	24.14	0.97

Figure 4(A-D) depicts the powdered substance diffraction by X-rays patterns of AS-6, AS-8, MAS-6, and also MAS-8. According to the powder XRD the structure, both aluminosilicates and Cu-aluminosilicates are generally made up of non-crystalline and additionally crystalline states.

A substantial even more diffraction patterns at 2θ = 30.69°-32.12° and 38.43°-38.78° which had been defined for Cu to be the monoclinic form of Copper oxide based on accordance using a typical JCPDS file (JCPDS file No. 048-1548) had been accessible in the scattering sequences of copper equipped aluminosilicate nanoparticles MAS-6 and MAS-8[22]. Grain size was calculated using Debye Scherer equation.

$$D = 0.9\lambda/\beta Cos\theta$$

Where

λ–Wavelength, β–full width half maximum (FWHM), θ–diffraction angle. AS-6, AS-8, MAS-6, MAS-8 of crystalite was found to be 11.4, 23.2, 12.8 and 32.8nm respectively.

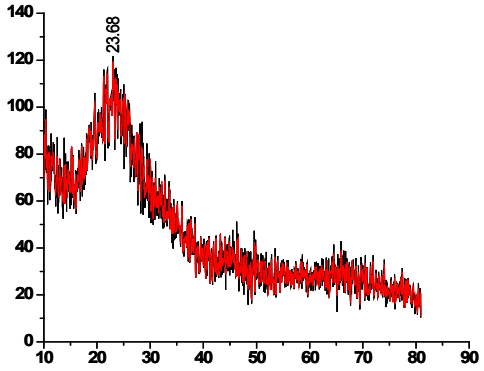

Fig. 4(a) XRD pattern of AS-6

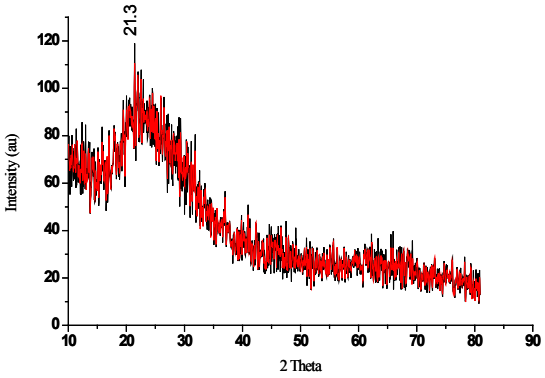

Fig. 4(b) XRD pattern of AS-8

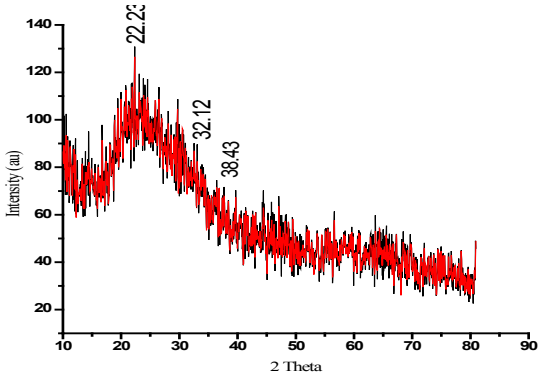

Fig. 4(c) XRD pattern of MAS-6

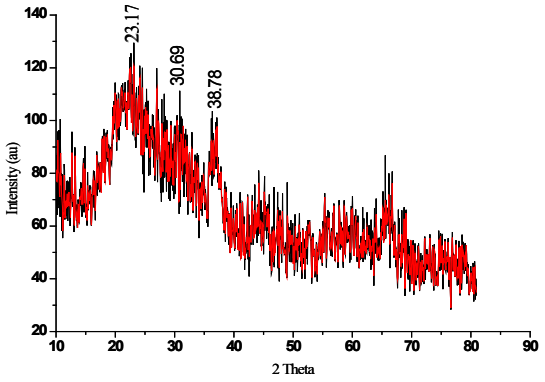

Fig. 4(d) XRD pattern of MAS-8

TGA analysis

TGA was used to evaluate the thermally attributes of MAS-6 and MAS-8 compounds (Fig. 5). At 450 and 650°C, the MAS-8 had fast weight reductions of 35 and 50%, accordingly, due to vaporization of ingested liquid and oxygen-containing functional categories. Once the surface temperature smashed 400°C, the mass of MAS-6 decreased little. A reduction in weight (4.5 wt %) was identified for MAS-8 materials at temperatures under 450°C owing to Al_2O_4 oxidation to α-Al_2O_3. During 450 and 650°C, there was substantial weight loss (26 wt %), which may be attributed to the breakdown and vaporization of several functional groups that contained oxygen on various portions of the MAS-8 surface. The outcomes showed that the MAS-8 compounds had excellent thermal resistance, which is most probably due to Cu^{2+} interaction within the aluminosilicate nanoparticles.

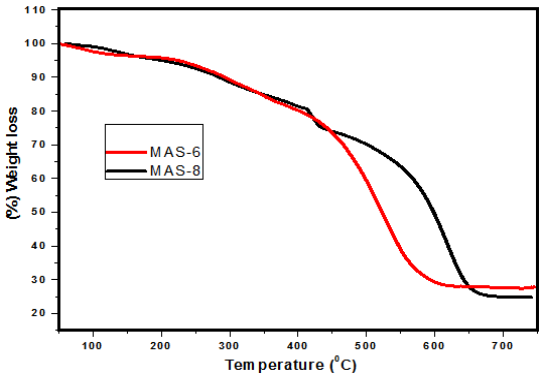

Fig. 5. TGA analysis of MAS-6 and MAS-8 composites by co-precipitation method

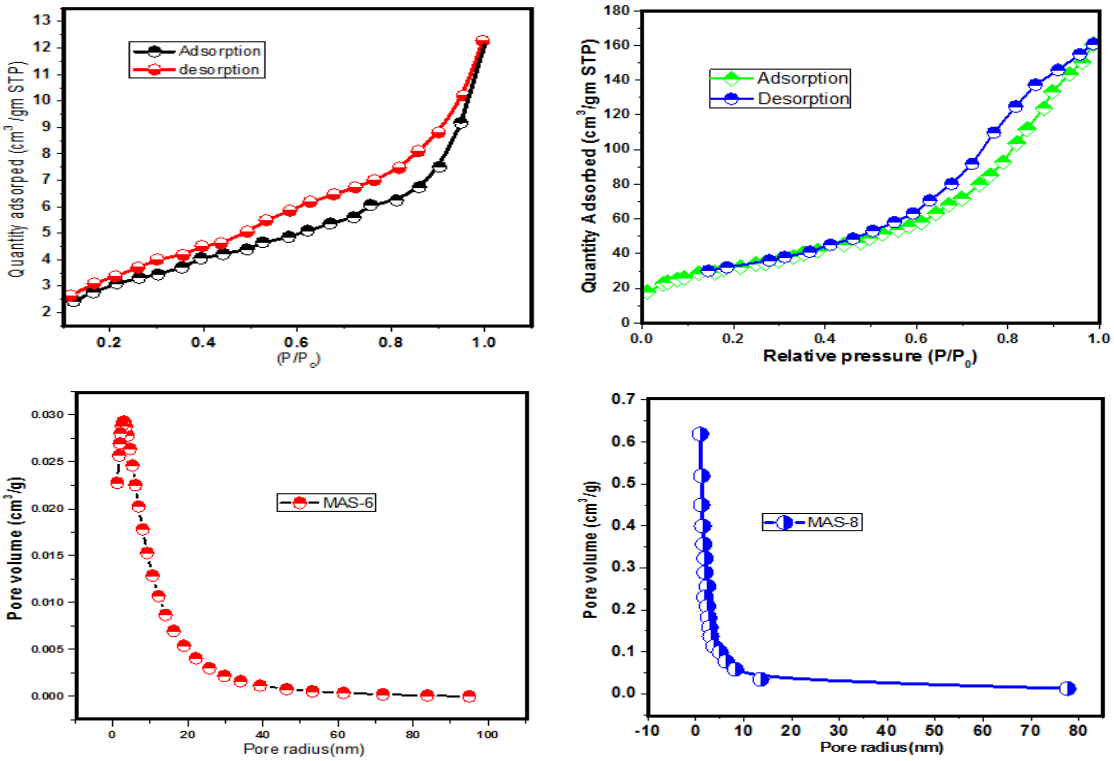

Fig. 6(a). BET isotherm MAS-6 (b) BET isotherm MAS-8 (c) pore distribution MAS-6 (d) pore distribution MAS-8 composites by co-precipitation method

The nitrogen adsorption-desorption equilibrium was used to compute the extent of the surface, porosity width, pore capacity, and distributions of pore sizes, while the outcomes are presented in Table 2. The BET Isotherms (Fig. 6) of MAS-6 and MAS-8 have been shown to have type-IV in character, confirming the mesoporous characteristics of both of those catalysts[23]. Copper aluminosilicate nanocomposites generated from aluminosilicate encourages heated up at 1000^{0}C and 1200^{0}C had an overall reduction through surface area as well as porosity when compared to an identical trigger acquired compared to the substrate heated at 800^{0}C, along with both of these characteristics could possibly be credited to extremely high humidity sintering process This would be consistent mitigating the reported rise in crystalline structure of support materials with the calcination temperature given the XRD analysis. Furthermore, the unstructured porosity generated after interstitial evacuation of the fluids in the lack of any extraneous patterns are responsible for the wide variety of pore dimensions found Figure 6 (c-d).

Table 2: Adsorption–desorption characteristics of MAS-6 & MAS-8

Catalyst	BET surface area (m^2 g^{-1})	BJH pore volume (cm^3 g^{-1})	BJH pore radius (nm)
MAS-6	184.29	0.2633	2.9
MAS-8	79.88	0.2138	3.4

Catalytic activity of Cu-aluminosilicate nanoparticles

Reduction of 4-nitrophenol to 4-aminophenol

Applying Cu-aluminosilicate nanocrystals to act as trigger, 4-nitrophenol (4-NP) was effectively transformed into 4-aminophenol (4-AP) with the assistance of hydrazine. After adding some of the hydrazine to the 4-NP solution containing Cu-aluminosilicate nanoparticles, the resulting transformation of 4-NP into 4-AP was demonstrated clearly. As the decomposition method carried on, the catalyst's supplementary using hydrazine caused the initial yellow color to shift to a colorless and clear substance.

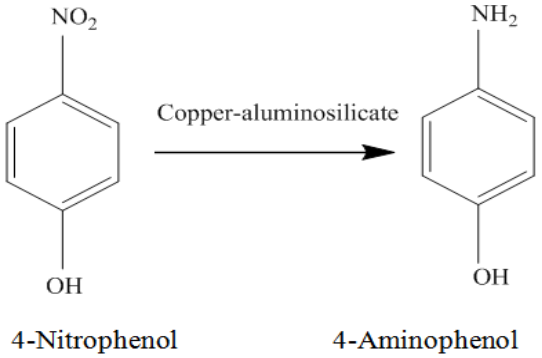

4-Nitrophenol 4-Aminophenol

Both of Cu-aluminosilicate nanocrystals have been examined for their effectiveness as catalysts through the ultraviolet-visible spectrochemical transformation of 4-Nitrophenol to 4-aminophenol. Not just the presence of hydrazine in fluid solutions may lead to the decrease. The Fig. 5 illustrates the results of the analysis. It illustrates the fact that a brand-new band around 340 nm forms as it acquires intensity over time, while the intensity of the 4-nitrophenol absorption band at λ_{max} 397 nm decreases over time. The synthesis of 4-aminophenol is what causes an additional band become visible at 340 nm. The two species' proportions can be estimated by their consumption intensity. The process of transformation of 4-nitrophenol to 4-aminophenol has been demonstrated by diminishing the level of absorption in the 397 nm band and raising its intensity in the 340 nm band[24,25].

Kinetic plot

Figures 8(a) and (b) depict the Catalytic breakdown kinetic of 4-NP. The catalytic break down of 4-NP is discovered to occur via a pseudo-first-order process[26,27].

$$\text{Ln } (C_0/C_t) = kt$$

Whereby C_0 denotes the original 4-NP content and C_t denotes the 4-NP concentration at time t (min^{-1}). The perceived response time variable is represented by the sign k. As seen in Fig. 8(a) and (b), k is 0.0331 for 4.8 mmol L1 of 4-NP and 0.0492 for 0.13 mmol L1 of 4-NP. The perceived rate of response steady drop at high 4-NP concentrations is most likely caused by the restricted activity sites of Cu aluminosilicate nanoparticles. The reduction occurs by the donation of an electron from $NaBH_4$ to the $–NO_2$ group. The *para mesomeric* donation is more effective than ortho mesomeric donation.

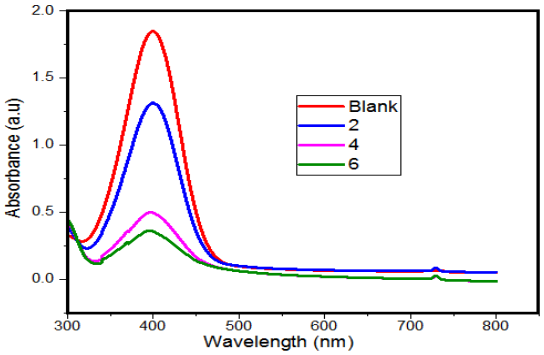

Fig. 7(a). UV-Vis spectra of catalytic activity of MAS-6 for reduction of 4-NP to 4 AP

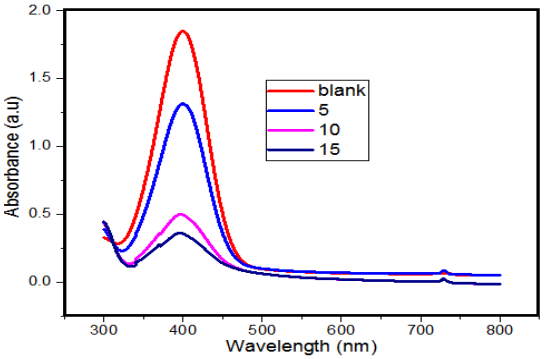

Fig. 7(b). UV-Vis spectra of catalytic activity of MAS-8 for reduction of 4-NP to 4 AP

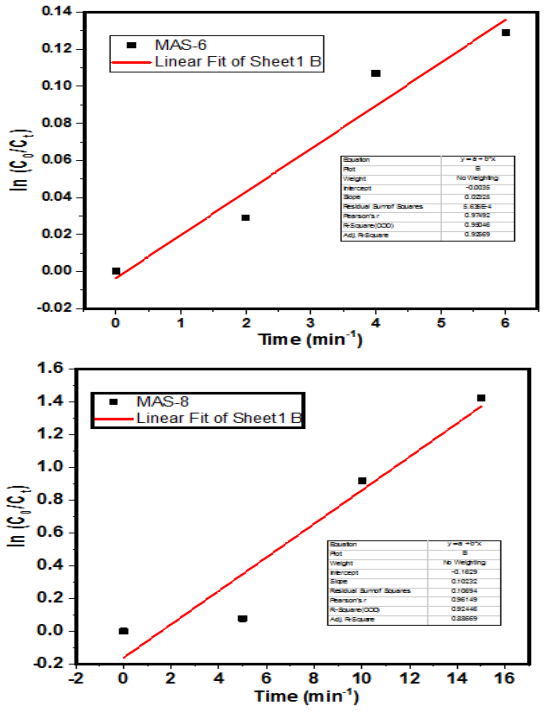

Fig. 8(a). kinetic plot of MAS-6 (b) kinetic plot of MAS-8 composites

Reduction mechanism

The Langmuir–Hinshelwood mechanism has been proposed by Wunder *et al.,* for investigating kinetically controlled surface catalytic reduction reactions of 4-nitrophenol by Cu-aluminosilicate nanostructures immobilized with porous structure. According to this mechanism, the metallic nanostructure provides a surface for the catalytic reduction process to take place. The BH_4^- ions adsorb on the surface of Cu-aluminosilicate and transfer hydrogen species to the surface of the Cu-aluminosilicate nanoparticles. At the same time, 4-nitrophenol also adsorbs on the surface and is reduced to 4-aminophenol by the BH_4^- ions. Finally, 4-aminophenol detaches to free the surface of the NPs for the next catalytic cycle to begin. The 1catalytic reduction of the nitrophenols with Cu-aluminosilicate is a heterogeneous catalytic reduction reaction.The heterogeneous catalytic reduction reaction can take place either by the L–H or the E–R (Eley–Rideal mechanism). In the case of the E–R mechanism, only one of the reactant molecules is adsorbed on the surface of the catalyst and reacts with the other reactant molecules. In the case of the L–H mechanism, both substrate molecules, nitrophenol and BH_4^-, get adsorbed on the surface of the catalyst and then, the reaction is occurs.

CONCLUSION

Without necessitate any kind of external framework, co-precipitation as well as calcination have been deployed to produce copper aluminosilicate nanostructures. The catalytic components that had been generated were analyzed by applying FT-IR, XRD, and SEM with EDX approaches. Cu-aluminosilicate nanoparticles' catalyst capabilities were determined for minimizing the conversion of 4-nitrophenol to 4-aminophenol with hydrazine at ambient temperature. The as-prepared Cu-aluminosilicate nanoparticles displayed a high the breakdown capacity for 4-NP, and the breakdown of 4-NP obeyed pseudo first-order dynamics. It was discovered that the Cu-aluminosilicate nanocomposites were an efficiently working and moderately durable trigger for converting 4-nitrophenol to 4-aminophenol.

ACKNOWLEDGEMENT

We thankful for St. Joseph's College in Tiruchirappalli for providing the FTIR and UV-Visible research for the centralized instrumentation facilities laboratory. Karunya University in Coimbatore has a lab with equipment for XRD and SEM study results with EDAX.

Conflict of interest

There is no conflict of interest for the author.

REFERENCES

1. Deka, P.; Bhattacharjee, D.; Sarmah, P.; Deka, R. C.; and Bharali, P.; Catalytic Reduction of Water Contaminant '4-Nitrophenol' over Manganese Oxide Supported Ni Nanoparticles, *Trends Asian Water Environ. Sci. Technol., Springer International Publishing, Cham.*, **2017**, 35–48.
2. Achamo, T.; and Yadav,O.P.; Removal of 4-Nitrophenol from Water Using Ag-N-PTridoped TiO_2 by Photocatalytic Oxidation Technique, *Anal. Chem. Insights.*, **2016**, 29–34.
3. Neal, R.D.; Inoue, Y.; Hughes, R.A.; and Neretina, S.; Catalytic Reduction of 4-Nitrophenol by Gold Catalysts: The Influence of Borohydride Concentration on the Induction Time, *J. Phys. Chem. C.*, **2019**, *123*, 12894–12901.
4. Abd Razak, N.F.; and Shamsuddin,M.; Catalytic reduction of 4-nitrophenol over biostabilized gold nanoparticles supported onto thioctic acid functionalized silica-coated magnetite nanoparticles and optimization using response surface methodology, *Inorg. Nano-Met. Chem.*, **2020**, *50*, 489–500.
5. Bogireddy, N.K.P.; Sahare,P.; Pal, U.; Méndez, S.F.O.; Gomez, L.M.; and Agarwal, V.; Platinum nanoparticle-assembled porous biogenic silica 3D hybrid structures with outstanding 4-nitrophenol degradation performance, *Chem. Eng. J.*, **2020**, *388*, 124237.
6. Sakurai,H.; and Murugadoss,A.; *Journal of Molecular Catalysis A: Chemical.*, **2011**, *341*, 1.doi.org/10.1016/j.molcata.2011.03.019.
7. Lee, S.J.; Yu, Y.; Jung, H.J.; Naik, S.S.; Yeon, S.; and Choi, M.Y.; Efficient recovery of palladium nanoparticles from industrial wastewater and their catalytic activity toward reduction of 4-nitrophenol, *Chemosphere.*, **2021**, *262*, 128358.

8. Viswanathan, B.; Sivasanker, S.; and Ramasamy, A. V.; Catalysis Principles and Applications, Narosa Publishing House., New Delhi., **2002**.
9. Padmaja, P.; K. Warrier, K.G.; Padmanabhan, M.; Wunderlich, W.; Berry, F.J.; Mortimer, M.; and Creamer, N.J.; *Materials Chemistry and Physics*., **2006**, *95*, 1. https://doi.org/10.1016/j.matchemphys.2005.05.044.
10. Vijayaraj, C.; Nedunchezhian, G.; Sofia Lawrence Mary, S.; *Eur.Chem.Bull*., **2023**, *12*, 413813.doi: 10.48047/ecb/2023.12.si4.12542023.29/05/2023
11. De Velasco-Maldonado, P. S.; Hernández-Montoya, V.; Montes-Morán, M. A.; *Applied Surface Science*., **2018**, *434*, 1193.doi.org/10.1016/j.apsusc.2017.11.023
12. Alghamdi, H.; Dakhane, A.; Alum, A.; Abbaszadegan, M.; Mobasher, B.; and Neithalath, N.; *Materials & Design*., **2018**, *152*, 10.https://doi.org/10.1016/j.matdes.2018.04.060.
13. Alonso,F.; Riente,P.; and Yus,M.; *Accounts of Chemical Research*., **2011**, *44*, 379.
14. Dhakshinamoorthy, A.; and Pitchumani,K.; *Tetrahedron Letters*., **2008**, *49*, 1818.doi.org/10.1016/j.tetlet.2008.01.061.
15. Alonso,F.; Riente, P.; Sirvent, J.A.; and Yus, M.; *Applied Catalysis A: General.,* **2010**, *378*, 42.doi.org/10.1016/j.apcata.2010.01.044.
16. Alonso, F.; Riente, P.; and Yus, M.; *Tetrahedron.,* **2009**, *65*, 10637.doi.org/10.1016/j.tet.2009.10.057.
17. Ciuffi, K. J.; Nassar, E. J.; Rocha, L. A.; daRocha, Z. N.; Nakagaki, S.; Mata, G.; Trujillano, R.; Vicente, M. A.; Korili, S. A.; Gil, A.; *Appl. Catal. A: Gen*., **2007**, *319*, 153–162.
18. Alonso, F.; Riente,P.; Yus,M.; *Acc. Chem. Res*., **2011**, *44*, 379–391.
19. Alonso,F.; Riente,P.; Sirvent,J.A.; Yus,M.; *Appl. Catal. A: Gen*., **2010**, *378*, 42–51.
20. Alonso, F.; Riente,P.; Yus,M.; *Tetrahedron*., **2009**, *65*, 10637–10643.
21. Lewandowska,A.; Monteverdi,S.; Bettahar,M.; Ziolek,M.; *J. Mol. Catal. A: Chem*., **2002**, *188*, 85–95.
22. Koltypin, Y.; Fernandez, A.; Rojas, T. C.; Campora, J.; Palma,P.; Prozorov, R.; Gedanken, A.; *Chem. Mater*., **1999**, *11*, 1331–1335.
23. Santamaria-Gonzalez, J.; Martinez-Lara, M.; Jimenez-Lopez, A.; *J. Chem. Soc. Faraday Trans*., **1997**, *93*, 493–497.
24. Kantam, M. L.; Rao, B. P. C.; Choudary, B. M.; Sreedhar, B.; *Adv. Synth. Catal.,* **2006**, *348*, 1970–1976.
25. Akkurt, M.; Roopan, S. M.; Khan, F. N.; Kumar, A. S.; Hathwar, V. R.; *Acta Crystallogr. E.,* **2010**, *66*, O1542-U1311.
26. Rauf, M. K.; Khan, F. N.; Roopan, S. M.; Hathwar, V. R.; Rajesh, R.; *Acta Crystallogr.* E., **2010**, *66*, O953–O3329.
27. Dayana Jeyaleela, G.; Rosaline Vimala, J.; Margrat Sheela, S.; Agila, A.; Stella Bharathy.; Divya.; *Orient. J. Chem*., **2020**, *36*, 3.